RSC Advances

PAPER

View Article Online
View Journal | View Issue

Cite this: *RSC Adv.*, 2025, **15**, 26216

Engineered acetylated inulin nanoparticles for enhanced oral insulin delivery: sustained release, structural stability, and *in vivo* efficacy†

Achmad Ramadhanna'il Rasjava, [ab] Neng Fisheri Kurniati[c] and Rukman Hertadi *[a]

Oral insulin administration is limited by enzymatic degradation and poor gastrointestinal absorption. This study aimed to develop a biopolymer-based nanocarrier using acetylated inulin (InAc) to improve the structural stability and oral bioavailability of insulin. Inulin was produced from *Salinivibrio* sp. GM01 and chemically modified *via* acetylation. Insulin-loaded InAc (InAc-Ins) nanoparticles were prepared and characterized for morphology, size, zeta potential, and encapsulation efficiency. *In vitro* insulin release was evaluated under simulated gastric (SGF) and small intestinal (SSIF) conditions. *In vivo* efficacy was determined through oral glucose tolerance tests (OGTT) in mice. The InAc-Ins nanoparticles were spherical with mean diameter of 349 ± 38 nm and high encapsulation efficiency (92.14%). Insulin release half-life were observed in 37.1 hours in SGF and 24.3 hours in SSIF conditions. Biophysical analysis revealed enhanced structural stability of encapsulated insulin, with increased half-life and activation energy for the secondary and tertiary structure denaturation. The secondary structure denaturation half-life increased to 195 min (SGF) and 231 min (SSIF), with denaturation enthalpy of 4.03 kcal mol^{-1} and 1.83 kcal mol^{-1}, respectively. Tertiary structure denaturation half-life were 765 min (SGF) and 919 min (SSIF), and denaturation enthalpy of 18.67 kcal mol^{-1} and 4.58 kcal mol^{-1}, respectively. OGTT results showed that orally administered InAc-Ins nanoparticles reduced blood glucose levels more effectively than free insulin, achieving 42.8% of subcutaneous insulin efficacy. InAc nanoparticles offer effective protection and sustained release of insulin under gastrointestinal conditions, enhancing its structural integrity and hypoglycemic efficacy. This platform presents a promising strategy for non-invasive oral insulin delivery.

Received 23rd May 2025
Accepted 16th July 2025

DOI: 10.1039/d5ra03627e

rsc.li/rsc-advances

Introductions

Diabetes mellitus (DM) is a chronic metabolic disorder characterized by impaired blood glucose regulation from either insufficient insulin secretion by pancreatic β-cells or the inability of cells to respond to insulin effectively.[1] As insulin plays an important role as an anabolic hormone, DM significantly disrupts the metabolism of carbohydrates, proteins, and fats, which can contribute to severe complications such as cardiovascular diseases, retinopathy, nephropathy, and neuropathy if not properly managed.[2] Current treatment strategies predominantly rely on subcutaneous insulin injections to regulate blood glucose levels. However, frequent administration through this route poses significant drawbacks, including pain, patient discomfort, and potential complications such as local tissue necrosis and infections.[3,4] In addition, insulin injections do not fully mimic the physiological pathway of insulin secretion, thus will impact its effectiveness in regulating blood glucose level.[5] As a result, there is an urgent need for a non-invasive, patient-friendly insulin delivery system to improve long-term diabetes management.

Among various alternatives, oral insulin administration offers a promising approach to enhance patient compliance while minimizing the risks associated with injections.[6] However, the bioavailability of oral insulin remains a major challenge due to biological barriers within the gastrointestinal (GI) tract. These include degradation by gastric acid and enzymatic proteolysis, as well as poor permeability across the intestinal epithelium.[7] Consequently, developing an efficient oral insulin delivery system that can protect insulin from degradation while facilitating its controlled release and absorption is crucial for advancing diabetes therapy.

Recent advances in nanotechnology have opened the way for innovative strategies in oral drug delivery, particularly for proteins and peptides like insulin. Nanocarrier-based delivery

[a]*Biochemistry and Biomolecular Engineering Research Division, Faculty of Mathematics and Natural Sciences, Bandung Institute of Technology, Bandung, West Java, Indonesia. E-mail: rhertadi@itb.ac.id*

[b]*Department of Chemistry, Faculty of Mathematics and Natural Sciences, Lambung Mangkurat University, Banjarbaru, South Kalimantan, Indonesia*

[c]*Department of Pharmacology-Clinical Pharmacy, School of Pharmacy, Bandung Institute of Technology, Bandung, West Java, Indonesia*

† Electronic supplementary information (ESI) available. See DOI: https://doi.org/10.1039/d5ra03627e

systems provide several advantages, such as enhanced protection against enzymatic degradation, improved intestinal permeability, and controlled drug release under physiological conditions.[8,9] A variety of nanomaterials, including polymeric nanoparticles, solid lipid nanoparticles, liposomes, and nanoemulsions, have been explored for insulin encapsulation to enhance its bioavailability.[10] Among these, polymeric nanoparticles derived from natural polysaccharides have demonstrated excellent biocompatibility, biodegradability, and stability in physiological environments.[11]

Inulin is a naturally occurring fructan polymer with versatile therapeutic applications such as a potential drug carrier due to its unique physicochemical properties and prebiotic benefits.[12] Composed of linear β-(2,1)-linked fructose units with a terminal glucose residue, inulin is resistant to hydrolysis by human digestive enzymes, thus allowing it to traverse the upper GI tract intact and will be disgusted by bifidobacterial in the lower GI tract.[13] This characteristic makes inulin an excellent candidate for targeted drug delivery, particularly for oral formulations requiring protection against harsh gastric conditions in which the drug then can be easily absorbed by the intestinal epithelium and transported to the bloodstream.[14] Previous studies have demonstrated that inulin-based nanoparticles effectively encapsulate and protect bioactive compounds, including proteins and enzymes, from degradation.[15,16]

Despite its advantages, the hydrophilicity of inulin poses a challenge for controlled drug release, as premature dissolution can lead to unintended drug leakage before reaching the target site. The solubility of inulin is primarily governed by its degree of polymerization (DP), with higher DP corelates with the reduced solubility.[15] An alternative approach to enhance inulin stability in water is by inserting hydrophobic groups to decrease its solubility.

In this study, acetic anhydride was employed to acetylate inulin. The acetylation of inulin increased the hydrophobicity of the nanoparticles, reducing gelation and significantly prolonging the drug release.[17] Acetylated inulin (InAc) also has been previously investigated as a drug delivery system for organic drugs or proteins and has demonstrated its potential as an encapsulation material, providing protection to the encapsulated substances.[16,17]

Compared to other biodegradable polymers, inulin-based nanoparticles offer the additional advantage of protecting insulin from premature degradation in the gastrointestinal tract due to their resistance to hydrolysis by human digestive enzymes.[18] Acetylated inulin also offers an advantage over some biodegradable polymers as its ester bonds can be hydrolyzed into inulin and non-toxic acetic acid without enzymatic catalysis.[16]

Another important factor in oral insulin formulation is ensuring insulin structural stability under varying physiological conditions. Protein stability is significantly influenced by environmental factors such as temperature, pH, and the presence of denaturants.[19] Since insulin is highly susceptible to degradation outside its optimal pH range, maintaining its native conformation is crucial for preserving its biological activity.[20] In protein stability studies, kinetic and thermodynamic approaches have been utilized extensively. One strategy for assessing protein stability is to use the protein denaturation half-life ($t_{1/2}$) and monitor the change in secondary and tertiary structures.[18,21] We propose an inulin-based nanoencapsulation material produced by the halophilic bacteria *Salinivibrio* sp. from Gili Meno, Lombok, for developing an oral insulin delivery system. The inulin nanoparticles utilized in the present study were designed to encapsulate and protect insulin conformation against GI conditions. We evaluated InAc capability to protect insulin using kinetic and thermodynamic approaches to examine insulin half-life and transition barrier before and after encapsulation.[18] Furthermore, *in vivo* analysis by glucose tolerance test was performed as a preliminary study to investigate the nanoparticles effectivity in reducing blood glucose levels.

Materials and methods

Materials

Inulin from chicory root (average degree of polymerization = 20), yeast extract, tryptone, Tween 80, sucrose, human recombinant insulin, ethanol (96% v/v), acetone (≥99% v/v), *N*,*N*-dimethylformamide (DMF) (≥99% v/v), sodium carboxymethylcellulose (Na-CMC), potassium chloride, hydrochloric acid, acetic acid, sodium acetate, sodium dihydrogen phosphate, sodium hydrogen phosphate, and sodium hydroxide were procured from Sigma-Aldrich, Singapore. Acetic anhydride (≥99% v/v) was obtained from Damao Chemicals, China. Bradford reagent was supplied by VWR Life Science, USA. The bacterial strain *Salinivibrio* sp. GM01 used in this study was obtained from the collection of the Biophysics and Biomaterials Research Group, Bandung Institute of Technology.

Production and characterization of inulin

The production and characterization of inulin from *Salinivibrio* sp. GM01 were conducted following our previously published method.[18] An aliquot of *Salinivibrio* sp. GM01 glycerol stock was cultured in 5 mL of Luria–Bertani (LB) medium containing 1% (w/v) tryptone, 0.5% (w/v) yeast extract, 7% (w/v) NaCl, and 2% (w/v) sucrose. The culture was incubated at 37 °C for 24 h with shaking at 150 rpm to obtain an overnight fresh culture. For inulin production, 2% (v/v) of the fresh culture was inoculated into 50 mL of LB medium supplemented with 10% (w/v) sucrose as a carbon source. The inoculated medium was incubated at 37 °C for 24 h with shaking at 150 rpm.

Following incubation, crude inulin was separated from the bacterial cells by centrifugation at 5000×*g* for 15 min. The supernatant containing inulin was collected and precipitated by the addition of three volumes of cold methanol at 4 °C, followed by incubation for 24 h. The inulin precipitate was recovered by centrifugation at 5000×*g* for 15 min and washed three times with 10 mL of sterile double-distilled water (ddH_2O). The purified inulin was then freeze-dried for 24 h and stored for further analysis.

Fourier-transform infrared (FTIR) spectroscopy was performed to confirm the functional groups present in the produced inulin by comparing its spectrum to that of standard

inulin. FTIR analysis was conducted using a Prestige 21 spectrometer (Shimadzu Corporation, Japan). For sample preparation, 10 mg of both the produced inulin and standard inulin were separately mixed with 10 mg of potassium bromide (KBr) powder until homogenous. The mixture was then compressed into a solid disc using a vacuum press. Spectra were recorded over a wavelength range of 400–4500 cm^{-1}.

Preparation and characterization of acetylated inulin

The acetylation of inulin was performed following a previously reported method with slight modifications.[16] To prepare the acetylated inulin (InAc), 0.25 g of In and 4 mg of sodium acetate were dissolved in 2.5 mL of DMF under stirring until complete dissolution. Subsequently, 1.0 mL of acetic anhydride was added dropwise to the solution. The reaction was carried out at 40 °C for 24 hours under 300 rpm. Upon completion of the reaction, the acetylated inulin was precipitated by the addition of 20 mL of sterile ddH_2O. The precipitate was collected by centrifugation at 5000×*g* for 15 minutes and washed three times with 10 mL of sterile ddH_2O. The collected product was then freeze-dried and stored for further analysis.

The chemical composition of InAc was analyzed using FTIR on a KBr disk following the aforementioned procedure. Proton nuclear magnetic resonance (^{1}H-NMR) spectroscopy analysis was conducted using an Agilent DD2 500 MHz NMR Spectrometer to determine the degree of acetylation (DA) of inulin. The analysis was carried out at a frequency of 500 MHz, with deuterated chloroform ($CDCl_3$) used as InAc solvent. The DA was determined by comparing the integral resonance peak intensities at 1.9–2.4 ppm and 3–6 ppm, which correspond to the methyl protons of the acetate group and the protons of the fructose backbone, respectively.[22] The number of acetyl groups per fructose unit was calculated from the integral of the resonance peak (IRP) at specific chemical shift (eqn (1)), and the DA were calculated using eqn (2).

$$\text{Acetyl group per fructose unit} = \frac{\text{IRP at } 1.9-2.4 \text{ ppm}/3}{\text{IRP at } 3-6 \text{ ppm}/7} \quad (1)$$

$$\text{Degree of acetylation(DA)} = \frac{\text{Acetyl group per fructose unit}}{\text{OH group per fructose unit}} \quad (2)$$

Preparation of inulin-insulin nanoparticles

The preparation of inulin-insulin nanoparticles followed our previously established method with slight modifications.[18] Briefly, 50 mg of inulin (In) or acetylated inulin (InAc) was dissolved in 10 mL of 96% (v/v) ethanol under continuous magnetic stirring for 10 minutes. Simultaneously, 0.5 mg of insulin was dissolved in 0.2 mL of 10 mM acetate buffer (pH 3.5). Following that, 50 μL of a 5% (w/v) aqueous Tween 80 solution was then added into the insulin solution. The two solutions were subsequently mixed and added dropwise into 20 mL of sterile distilled water under stirring at 17 800 rpm for 10 minutes using an Ultra-Turrax homogenizer to obtain inulin-insulin nanoparticles. The nanoparticles were collected *via* centrifugation at 5000×*g* for 30 minutes, followed by washing the nanoparticles with 1 mL of sterile distilled water. Finally, the nanoparticles were freeze-dried for 24 hours. Blank inulin nanoparticles were prepared in an identical manner but without insulin, served as controls in subsequent experiments. The encapsulation efficiency of inulin-insulin nanoparticles was calculated as the ratio of insulin encapsulated within the nanoparticles to the total amount of insulin added using eqn (3), them expressed as a weight-to-weight (w/w) percentage.[22]

$$\text{Encapsulation effieciency(\%EE)} = \frac{\text{Initial} - \text{Free insulin}}{\text{Initial insulin}} \times 100\% \quad (3)$$

For clarity in the further characterization, the blank inulin nanoparticles were designated as In-B NPs, while inulin-encapsulated insulin nanoparticles (non-acetylated) were referred to as In-Ins NPs. Similarly, blank acetylated inulin nanoparticles were labeled as InAc-B NPs, and acetylated inulin-encapsulated insulin nanoparticles were labeled as InAc-Ins NPs.

Drug loading capacity and maximum loading capacity

In this study, drug loading capacity (DLC) refers as the actual amount of insulin encapsulated per total weight of insulin-loaded NPs reflecting the percentage of insulin content in the final formulation. DLC was determined from the standard formulation using 0.5 mg of insulin mixed with 50 mg of InAc. DLC value was then calculated using eqn (4).

$$\text{DLC}(\%) = \frac{\text{Encapsulated insulin(mg)}}{\text{Insulin} - \text{loaded NPs weight(mg)}} \quad (4)$$

Maximum loading capacity (LC_{max}) was determined in a separate saturation experiment to quantify the maximum insulin amount that could be retained per mg of encapsulating material, regardless of the final nanoparticle mass. To determine this, the insulin-loaded NPs were prepared using 50 mg of encapsulation material and excess amount of insulin solution (10 mg mL^{-1}) to allow saturation. After nanoparticle formation and recovery, the unencapsulated insulin remaining in the supernatant was quantified using the Bradford assay. The LC_{max} was then calculated using eqn (5).

$$LC_{max}\ (\mu g/mg) = \frac{\text{Encapsulated insulin } (\mu g)}{\text{Encapsulated material weight (mg)}} \quad (5)$$

Characterization of inulin-insulin nanoparticles

The physicochemical characteristics of In-Ins and InAc-Ins NPs were analyzed through morphological evaluation, size distribution, surface charge determination, and elemental composition analysis. Morphological characterization was performed using Hitachi Model H-9500 high-resolution transmission electron microscopy (HR-TEM) (Hitachi, Japan) operated at an acceleration voltage of 300 kV. Prior to imaging, nanoparticles samples were deposited onto a carbon-coated copper grid and observed at 2 000 00× magnification and compared with In-B or

InAc-B NPs to evaluate structural differences. Particle size, polydispersity index (PDI), and zeta potential were measured using dynamic light scattering (DLS) with a Horiba SZ-100 particle size analyzer (Horiba, Japan) at 25 °C. Nanoparticles samples (10 mg) were dispersed in 1 mL of phosphate-buffered saline (PBS, pH 7.0). The data were analyzed using the instrument built-in software. The elemental composition of the nanoparticles was assessed by energy dispersive spectroscopy (EDS) coupled with a SU3500 scanning electron microscope (Hitachi, Japan) under a 15 kV high-vacuum condition. Prior to EDS analysis, samples were sputter-coated with gold using an MC1000 Ion Sputter Coater (Hitachi, Japan) at 10 mA for 90 seconds under an argon gas.

Kinetics and thermodynamics study

***In vitro* release study of inulin-insulin nanoparticles.** The *in vitro* release profile of insulin from inulin-insulin nanoparticles was evaluated under simulated gastric and intestinal conditions. A total of 50 mg of inulin-insulin nanoparticles were dispersed in 10 mL of simulated gastric fluid (SGF) and simulated small intestinal fluid (SSIF). SGF and SSIF were prepared as described in previous studies.[23] SGF was prepared using 200 mM HCl–KCl buffer without the addition of pepsin. The pH of the solution was then adjusted to pH 1 using 1.0 M HCl. Similarly, SSIF without enzymatic components was prepared using 50 mM phosphate-buffered saline (PBS), with the pH adjusted to 7.0 using either 0.1 M HCl or 0.1 M NaOH. The samples were incubated at 25 °C (mimicking ambient temperature) and 37 °C (mimicking physiological temperature) under continuous agitation at 150 rpm for a duration of 4 hours, simulating the typical gastric retention time.[24] The release of insulin in both samples was measured by taking samples at specific time intervals and the nanoparticles were separated *via* centrifugation to remove any suspended nanoparticles. The insulin concentration in the supernatant was quantified using the Bradford assay at a wavelength of 595 nm.[25] The cumulative percentage of released insulin was then plotted as a function of time to generate the release profile under SGF and SSIF conditions.

Insulin secondary and tertiary structure stability. The conformational stability of insulin encapsulated in the nanoparticles was assessed under four different conditions: pH 1, pH 7, 25 °C, and 37 °C, and compared with free-state insulin. The structural stability was analyzed using circular dichroism (CD) spectroscopy to evaluate the secondary structure and fluorescence spectroscopy to assess the tertiary structure.

For secondary structure analysis, a CD spectrophotometer (J-1500, Jasco, Japan) was operated in the wavelength range of 190–220 nm, with a scanning rate of 50 nm min^{-1}. The percentage of α-helices was determined at various time intervals with three replicates per condition. The obtained values were plotted over time to generate a denaturation curve, which was used to calculate the rate constant (k), half-life ($t_{1/2}$), and activation energy (E_a) for insulin denaturation.[21]

Tertiary structure stability was analyzed using a fluorescence spectrophotometer (RF-5310 PC, Shimadzu, Japan) with an excitation wavelength of 274 nm and an emission wavelength range of 290–400 nm.[26] Fluorescence intensity was recorded at different time intervals under identical conditions. The obtained data were used to determine the rate constant (k), half-life ($t_{1/2}$), and activation energy (E_a) for tertiary structure denaturation. For both secondary and tertiary structure stability, the enthalpy activation ($\Delta H^{\ddagger}_{D-N}$) was calculated using the following equations were applied.

$$k = \frac{\ln 2}{t_{1/2}} \tag{6}$$

$$k = A\, e^{-E_a/RT} \tag{7}$$

$$\Delta H^{\ddagger}_{D-N} = E_a - RT \tag{8}$$

where A represents the pre-exponential factor, R is the ideal gas constant ($R = 1.987$ cal K^{-1} mol^{-1}), and T is the absolute temperature in Kelvin. These equations were used to determine the enthalpy activation associated with both the helix-to-coil transition in the secondary structure and the tertiary structure unfolding of insulin.

Oral glucose tolerance test. The *in vivo* study was conducted using healthy male Swiss Webster mice (25–30 g, 8 weeks old), obtained from the School of Pharmacy, Bandung Institute of Technology. The animals underwent a two-week acclimatization period with ad libitum access to a standard chow diet and water. Food consumption was monitored daily by calculating the difference between the supplied and remaining chow. Body weight was recorded every three days using an electronic balance. All mice were housed under standard laboratory conditions with a 12-hour light/12-hour dark cycle.[27]

To evaluate glucose tolerance, an oral glucose tolerance test (OGTT) was performed using groups of five mice per treatment condition. Following an overnight fasting period, the mice were administered either subcutaneous (SC) insulin (2.5 IU kg^{-1}, SC), In-B NPs (750 mg kg^{-1}, oral), InAc-B NPs (750 mg kg^{-1}, oral), In-Ins NPs (50 IU kg^{-1}, oral), InAc-Insulin NPs (50 IU kg^{-1}, oral), or free-state (FS) insulin (50 IU kg^{-1}, oral), each dispersed in 1 mL of 0.25% (w/v) sodium carboxymethyl cellulose (Na-CMC). The control group was treated 1 mL of 0.25% (w/v) Na-CMC. Immediately after administration, the mice were orally challenged with glucose (3 g kg^{-1} body weight). Blood samples were collected from the tail vein at predetermined time points (0, 30, 60, 90, 120, and 150 minutes) post-glucose administration, and blood glucose levels were measured using an EasyTouch glucometer (Bioptik Technology Inc., Taiwan). The OGTT results were expressed as blood glucose concentration over time, and the area under the curve (AUC) was calculated using the trapezoidal method to assess glucose tolerance quantitatively.[18]

Additionally, a dosage variation study was conducted exclusively for InAc-Ins NPs, as they demonstrated the most promising glucose-lowering effect in preliminary assessments. The dosage variation study included three groups receiving different doses of InAc-Ins NPs: 50, 100, and 200 IU kg^{-1} body weight, designated as D1, D2, and D4, respectively. The OGTT procedure was replicated for these groups to assess the dose-dependent effect of InAc-Ins NPs on glucose regulation.

All experimental procedures adhered to the Guidelines on Animal Care and Use for Education and Research Purposes of the School of Pharmacy, Bandung Institute of Technology (Protocol No. 004/SF ITB/2015). Ethical approval for the animal experiments was granted by the Universitas Padjadjaran Research Ethics Committee under Protocol No. 1294/UN6. KEP/EC/2023.

Statistical analysis. All experiments were performed in triplicate, unless otherwise stated. Data are presented as mean ± standard deviation (SD). For comparison between two groups, an unpaired two-tailed Student's *t*-test was used. For multiple group comparisons, one-way analysis of variance (ANOVA) followed by Tukey's post hoc test. Differences were considered statistically significant at p-value < 0.05.

Results and discussion

Characterization of inulin and acetylated inulin

The bacterial inulin was successfully produced by halophilic bacterium *Salinivibrio* sp. GM 1 following the previously described method and subsequently characterized using Fourier-transform infrared (FTIR) spectroscopy.[18,28] The resulting FTIR spectrum was then compared with inulin extracted from chicory root (Fig. 1A). The characteristic absorption bands observed at 3384, 2916, 1637, and 1439 cm^{-1} were attributed to O–H stretching vibrations, C–H stretching vibrations, –OH bending vibrations, and C–H bending, respectively, representing distinct functional groups in polysaccharides.[29] The bands at 1122 and 1022 cm^{-1} corresponded to the C–O–C and C–O stretching vibrations, characteristic of the furanose ring. Additionally, the absorption band at 924 cm^{-1} confirmed the presence of D-glucopyranosyl units.[30] The spectral features of the bacterial inulin (In) closely matched those of chicory inulin, confirming its successful production.

The schematic reaction of inulin acetylation is shown in Fig. 1B. The FTIR spectrum of InAc exhibited similar absorption bands to those of In (Fig. 1A), with notable shifts in peak positions. These spectral changes were attributed to reduced hydrogen bonding and the introduction of additional C–H bonds due to the incorporation of acetyl ($–CH_3$) groups. The most prominent spectral differences in InAc included the appearance of a new absorption peak at 1696 cm^{-1}, corresponding to C=O stretching of the ester group, and a decreased intensity at 3408 cm^{-1}, indicating the substitution of hydroxyl (–OH) groups with acetyl groups. Additional characteristic peaks at 1332 cm^{-1} ($–CH_3$ bending) and 1194 cm^{-1} (–C–O bending) further confirmed the presence of acetyl groups.[22] These spectral features verified the successful acetylation of inulin while retaining its essential structural characteristics. These spectral changes also consistent with previously reported findings on acetylated inulin derivatives utilized in drug delivery systems, which exhibited similar distinct peak shifts in the same wavenumber regions.[31,32]

For a more detailed structural analysis, proton nuclear magnetic resonance (^{1}H-NMR) spectroscopy was employed to determine the degree of acetylation and the number of acetyl groups substituted per fructose unit.[22] The ^{1}H-NMR results indicated an average of 2.36 ± 0.08 acetyl groups per fructose unit, corresponding to a DA of 78.71 ± 2.57%. The ^{1}H-NMR spectra are provided in Fig. S1,† further substantiating the structural modification of inulin through acetylation. The ^{1}H-NMR spectrum of InAc confirms the successful chemical modification. A characteristic singlet observed at approximately 2.05 ppm corresponds to the methyl protons ($–CH_3$) of the acetyl groups, indicating the substitution of hydroxyl groups with acetyl groups. In addition, broad signals appearing between 3.4 and 5.6 ppm were attributed to the ring protons of the inulin backbone, primarily at the C2–C6 positions of the β-(2,1)-linked fructofuranose units. The presence of the acetyl peak alongside these downfield-shifted sugar resonances confirms the esterification reaction and is consistent with prior reports on acetylated polysaccharides used for intestinal delivery applications.[22,31] This high level of acetylation significantly alters the physicochemical properties of inulin by enhancing its hydrophobicity, thereby contributing to the formation of a more compact and water-resistant nanoparticle matrix.[33] Such DA value is generally classified as high, which has been associated with modifications in biopolymer functionality for reduced gelatinization, suppressed retrogradation, and improved structural integrity under physiological conditions.[34]

Characterization of inulin-insulin nanoparticles

Morphology analysis. The morphology of blank and insulin-loaded inulin nanoparticles was examined using high-

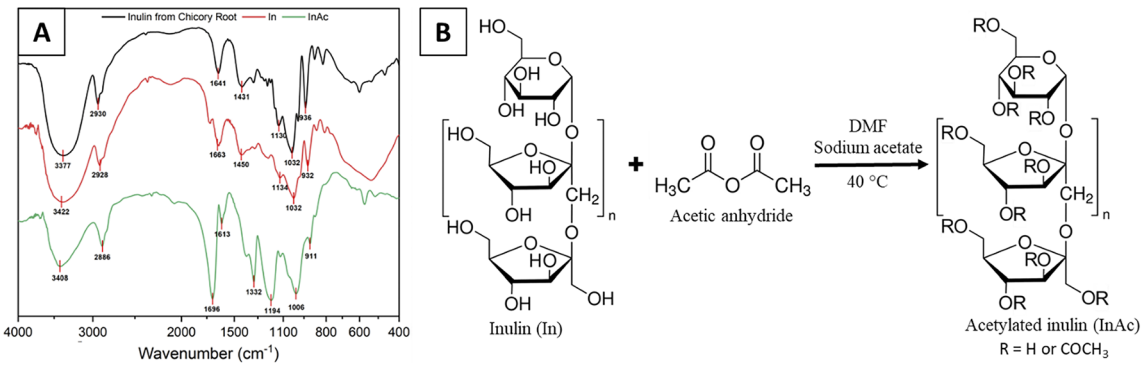

Fig. 1 (A) FTIR spectra of inulin from chicory root (black line), In (red line), and InAc (green line). (B) Schematic representation of the acetylation reaction of inulin.

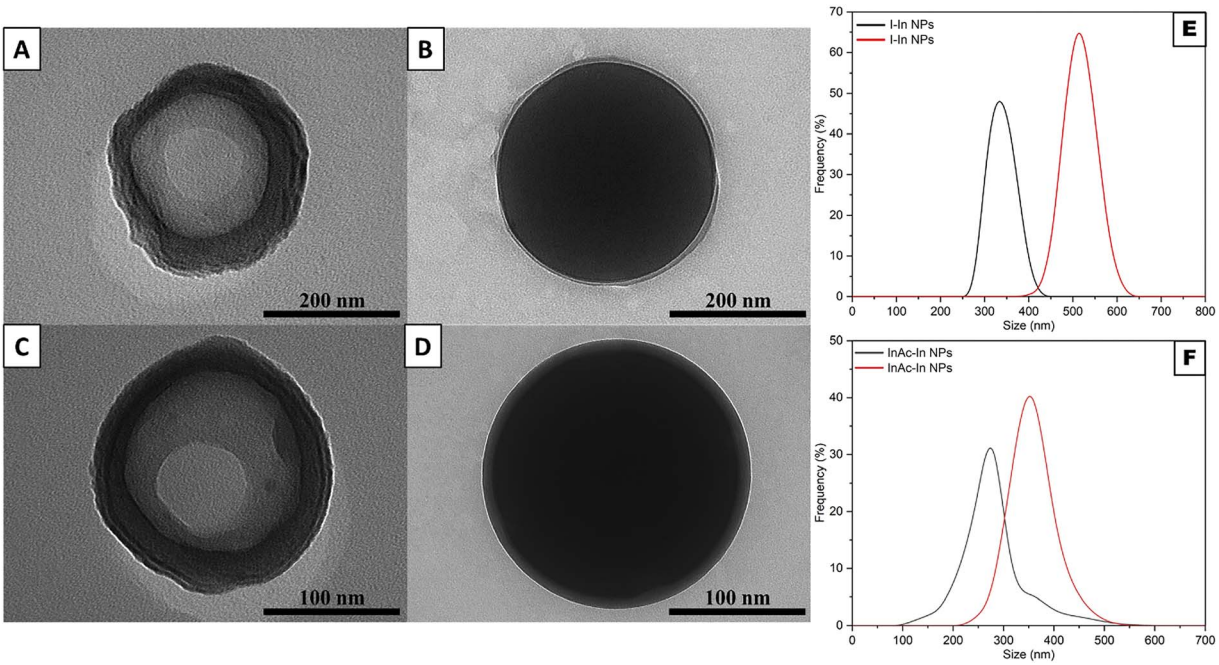

Fig. 2 The tem images of (A) In-B NPs, (B) In-Ins NPs, (C) InAc-B NPs, and (D) InAc-Ins NPs, and the particle sizes distribution of (E) In-B NPs and In-Ins NPs, and (F) InAc-NPs and InAc-Ins NPs.

resolution transmission electron microscopy (HR-TEM) (Fig. 2A–D). The HR-TEM images revealed that In-B NPs displayed a spherical shape with a distinct central cavity (Fig. 2A). Meanwhile, In-Ins NPs maintained a similar morphology, but with the cavities appeared to be filled with insulin molecules, as indicated by the darker color as the density increased as shown in Fig. 2B.[35] InAc-B NPs and InAc-Ins NPs displayed similar morphologies the In-B and In-Ins NPs (Fig. 2C and D), albeit with a reduced particle size.

TEM and PSA analysis revealed that both In and InAc NPs maintained spherical morphology, but acetylation significantly reduced particle size (Fig. 2). Acetylation resulted in a significant reduction in particle size, as observed in the smaller dimensions of InAc-B NPs compared to InB NPs (Fig. 2A and C). This result is consistent with previous studies demonstrating that acetylation can effectively reduce particle size and droplet diameter in nanomaterial-based formulations.[36,37] The introduction of acetyl groups disrupts intermolecular hydrogen bonding and increases surface hydrophobicity, promoting tighter molecular packing and limits particle aggregation during nanoparticle formation.[37]

Although the molecular weight of inulin was not directly measured in this study, the acetylation process likely created a mildly acidic environment due to the generation of acetic acid. This condition might lead to partial hydrolysis of the glycosidic bonds, resulting in limited depolymerization of the inulin backbone.[38,39] Acetylation also decreases intermolecular interactions by replacing hydroxyl groups with non-ionizable ester groups, reducing steric hindrance and allowing the nanoparticles to form smaller particles. The increased hydrophobicity of InAc also promotes self-assembly into denser structures.[40] The presence of internal pores within the nanoparticle structure may facilitate insulin entrapment by enabling diffusion of insulin molecules into the NPs core.[41]

Particle size and surface charge analysis. The particle size distribution of the nanoparticles was determined using a particle size analyzer (PSA) at 25 °C and pH 7. Table 1 summarizes the physicochemical properties of various polysaccharide-based nanoparticles, including both newly synthesized acetylated inulin nanoparticles and reference systems reported in previous studies.[18,21] Data for In-B and In-Ins NPs were reproduced from our prior work[18] to provide a direct comparison under equivalent experimental conditions. Levan-based formulations were included to benchmark against another fructan-type polymer widely investigated for insulin encapsulation.[21]

Insulin-loaded NPs exhibited increased particle sizes relative to their blank counterparts. In-B and IN-Ins NPs displayed mean diameters of 338 ± 44 nm and 416 ± 32 nm, respectively (Fig. 2E), while InAc-B and InAc-Ins NPs had mean diameters of 264 ± 58 nm and 349 ± 38 nm, respectively (Fig. 2F). This results suggest successful encapsulation of insulin within the NPs matrix.[18] The particle size of InAc-Ins NPs observed in this study (349 ± 38 nm) closely corresponds to that of previously reported acetylated levan-insulin nanoparticles (LevAc-Ins NPs), which exhibited a mean diameter of 335 ± 31 nm.[21] Although both systems underwent similar acetylation procedures, the InAc-Ins NPs displayed slightly larger mean diameter size (Table 1). This difference is likely attributable to fundamental differences in the molecular architecture of the base polysaccharides. Inulin is composed by linear β(2 → 1)-linked fructose units, exhibits greater conformational rigidity and a higher persistence length than levan, which is composed of more branched β(2 → 6)-linked fructose units.[42] As demonstrated by molecular dynamics

Table 1 Summary of the nanoparticle physical properties

Sample	Encapsulation efficiency (%)	DLC (% w/w)	LC_{max} (μg insulin/mg polymer)	Particle size (nm)	Polydispersity index	Zeta potential	Sources
Levan-blank NPs	—	—	—	281 ± 23	0.308	−15.20 ± 1.04	Kurniawati *et al.*[21]
Levan-Ins NPs	78.64	7.79	117.68 ± 0.68	319 ± 19	0.580	−10.80 ± 1.34	Kurniawati *et al.*[21]
LevAc-blank NPs	—	—	—	266 ± 35	0.639	−11.60 ± 1.21	Kurniawati *et al.*[21]
LevAc-Ins NPs	88.30	8.74	133.97 ± 0.23	335 ± 31	0.660	−10.70 ± 1.06	Kurniawati *et al.*[21]
InB NPs	—	—	—	338 ± 44	0.404	−14.26 ± 1.26	Rasjava *et al.*[18]
In-Ins NPs	87.04 ± 3.01	8.62% ± 0.30	115.67 ± 0.34	416 ± 32	0.359	−8.74 ± 1.02	Rasjava *et al.*[18]
InAc-B NPs	—	—	—	264 ± 58	0.386	−12.53 ± 1.32	This work
InAc-Ins NPs	92.14 ± 1.18	9.12 ± 0.12	138.21 ± 1.76	349 ± 38 nm	0.375	−9.41 ± 1.06	This work

simulations, inulin tends to adopt extended conformations and local 2_1-helical motifs, whereas levan displays enhanced chain flexibility and lower energy barriers for conformational rearrangement.[42] Despite these differences, both InAc- and LevAc-based nanoparticles fall within the optimal size range of 200–600 nm, which is generally considered favorable for oral absorption *via* the intestinal epithelium.[21]

Zeta potential analysis revealed the surface charge characteristics of the nanoparticles. Zeta potential measurements provided insights into the surface charge of the nanoparticles. The InAc-B NPs exhibited a zeta potential of −12.53 ± 1.32 mV, which decreased to −9.41 ± 1.06 mV upon insulin encapsulation in the InAc-Ins NPs. The decrease in zeta potential following insulin encapsulation is attributed to charge compensation by the insulin molecules, which interact with the nanoparticle surface through their charged amino acid residues. Additionally, acetylation altered the surface charge of the nanoparticles by replacing hydroxyl groups with non-ionizable ester groups, thereby reducing the overall negative charge compared to non-acetylated inulin nanoparticles.[40]

In addition to favorable size and surface charge characteristics, the InAc-Ins NPs demonstrated an exceptionally high encapsulation efficiency (% EE) of 92.14 ± 1.18%, which surpassed In-Ins (87.04 ± 3.01%) and all levan-based systems (Table 1). This high % EE reflects the efficient entrapment of insulin within the acetylated polymer matrix. The DLC for InAc-Ins NPs was calculated at 9.12 ± 0.12%, higher than In-Ins (8.62 ± 0.12%), LevAc-Ins (8.74%), and Levan-Ins NPs (7.79%). These values indicate that InAc not only encapsulates insulin efficiently but also allows greater insulin content per nanoparticle mass. Moreover, the maximum loading capacity (LC_{max}) revealed that InAc-Ins NPs could retain up to 138.21 ± 1.76 μg insulin/mg InAc, higher than LevAc-Ins (133.97 μg mg^{-1}), In-Ins (115.67 μg mg^{-1}), and Levan-Ins NPs (117.68 μg mg^{-1}). These enhancement is primarily attributed to the increased hydrophobicity and reduced solubility of acetylated inulin and levan, which create a more compact and water-resistant matrix during nanoparticle formation.[43]

Elemental composition analysis. The encapsulation of insulin within the nanoparticles was further confirmed through elemental composition analysis using energy-dispersive X-ray spectroscopy (EDS). The elemental composition of InAc-B NPs was analyzed before and after insulin loading (Fig. 3A and B). Prior to insulin addition, the InAc-B NPs primarily contained carbon (C) and oxygen (O), with nitrogen (N) and sulfur (S) being undetectable. Following insulin encapsulation (InAc-Ins NPs), the presence of N and S increased significantly, corresponding to the amine and thiol groups present in insulin. Simultaneously, the relative weight percentage of C and O decreased, further supporting the successful incorporation of insulin within the nanoparticle matrix.[44]

Insulin release study. The stability and release profile of insulin from the developed inulin-based nanoparticles (In-Ins and InAc-Ins NPs) were evaluated under simulated gastrointestinal conditions. The insulin release profiles from In-Ins and InAc-Ins nanoparticles demonstrated different behaviors under both SGF and SSIF conditions (Fig. 4 and S2†).

The In-Ins NPs showed a rapid, pH-independent burst release in both SGF and SSIF, with insulin release half-life of approximately 60 ± 1 minutes in SGF and 58 ± 2 minutes in SSIF.[18] This results is consistent with previous studies on inulin from chicory root used as an encapsulation material.[17,43] This release behavior is attributed to the hydrophilic nature of unmodified inulin, which promotes fast solvent penetration and insulin diffusion (Fig. 4A). In contrast, InAc-Ins NPs exhibited significantly prolonged release, with insulin release half-life of 37.1 ± 2.9 hours in SGF and 24.3 ± 1.5 hours in SSIF. This sustained release is attributed to the increased hydrophobicity conferred by acetylation, which reduces matrix swelling and slows insulin diffusion (Fig. 4B). This behavior is in agreement with previous findings on the encapsulation of mesalamine using acetylated inulin.[43] The prolonged insulin release from InAc-Ins nanoparticles is attributed to the increased hydrophobicity induced by acetylation, which limits matrix disintegration and swelling.

The comparable release profiles in both SGF and SSIF indicate a pH-independent and stable delivery system. These results demonstrate that acetylated inulin enables controlled and sustained insulin release. These results also indicate that modifying inulin with varying DA *via* acetic anhydride treatment allows for controlled release rate of insulin, offering potential for sustained drug delivery applications.[31]

Analysis of insulin structural stability in nanoparticles. The structural stability of insulin encapsulated within inulin-insulin

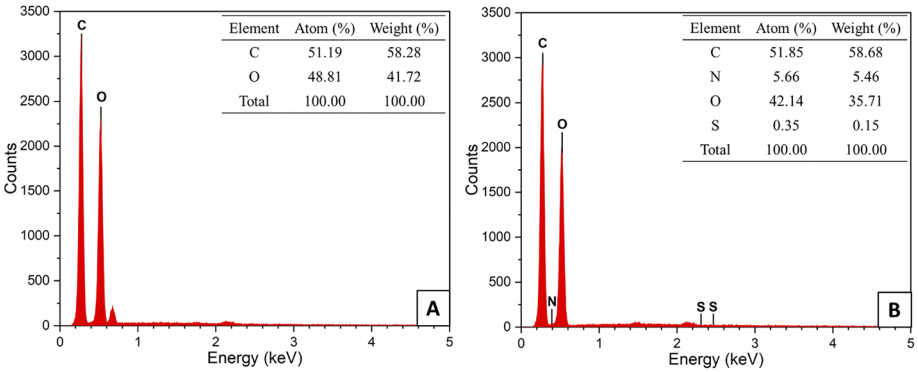

Fig. 3 EDS result for (A) InAc-B NPs and (B) InAc-Ins NPs.

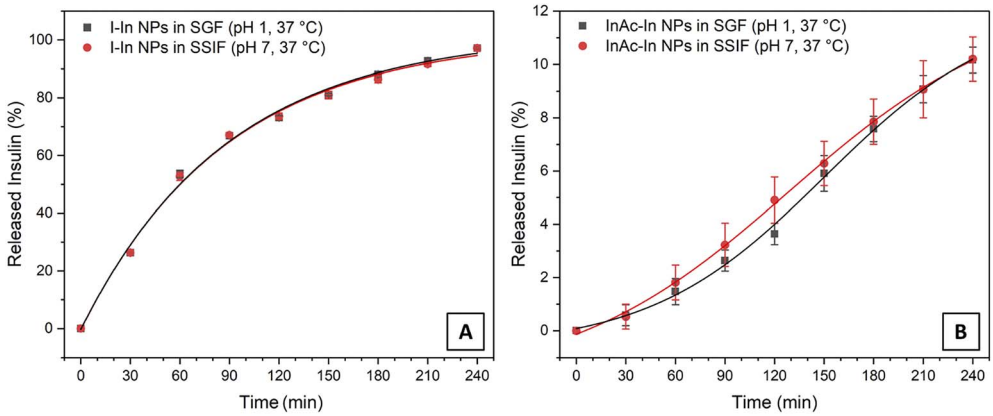

Fig. 4 Insulin release profiles from (A) In-Ins NPs and (B) InAc-Ins NPs in SGF (pH 1) and SSIF (pH 7) at 37 °C over a four-hours incubation period.

nanoparticles was assessed at pH 1 and pH 7 using circular dichroism (CD) and fluorescence spectroscopy at 37 °C. CD spectroscopy was employed to evaluate the preservation of the insulin secondary structure by quantifying the percentage reduction in helicity. Meanwhile, fluorescence spectroscopy was utilized to assess the stability of the insulin tertiary structure by measuring changes in fluorescence intensity due to quenching effects. Our study takes a biophysical approach to assess the stability of encapsulated insulin by employing kinetic and thermodynamic analysis.[18,21]

Insulin secondary structure stability in nanoparticles. Circular dichroism (CD) spectroscopy was performed to assess the structural integrity of both free and encapsulated insulin by evaluating the preservation of the insulin secondary structure by quantifying the insulin helical content at pH 1 and pH 7 at 37 °C. The CD spectral analysis demonstrated that encapsulation with InAc did not result significant alterations in the secondary structure of insulin (Fig. 5A). Both free and encapsulated insulin exhibited characteristic α-helical peaks at 208 and 222 nm, indicating the preservation of insulin native conformation. These findings are consistent with previous studies on insulin encapsulated with polyhedral oligosilsesquioxane, which also reported no significant conformational changes upon encapsulation.[45]

The analysis revealed that FS Insulin underwent a faster loss of helical content compared to the encapsulated insulin under both conditions (Fig. 5B, C and S3†). Insulin encapsulation with InAc significantly slowed the secondary structure denaturation rate and extending the half-life of insulin by approximately 1.5-fold compared to FS insulin (Table 2). For FS insulin, E_a values were 2.08 ± 0.02 kcal mol^{-1} at pH 1 and 1.14 ± 0.25 kcal mol^{-1} at pH 7. Meanwhile, InAc-Insulin NPS exhibited higher Ea values, with 4.64 ± 0.21 kcal mol^{-1} at pH 1 and 2.45 ± 0.18 kcal mol^{-1} at pH 7, indicating increased structural stability upon encapsulation. Insulin encapsulation with InAc also resulted in a significant increase in denaturation transition enthalpy ($\Delta H^{\ddagger}_{D-N}$), with values of 2.57 ± 0.15 kcal mol^{-1} at pH 1 and 1.31 ± 0.21 kcal mol^{-1} at pH 7 (Table 2).

The increase in transition enthalpy indicates that encapsulated insulin requires more energy to undergo denaturation, confirming its improved resistance to degradation compared to the free form. These results is in agreement with previous findings, where increased activation energy and transition enthalpy upon encapsulation correlated with improved protein stability.[21]

The comparative data in Table 2 demonstrate that inulin- and levan-based carriers provide different degrees of stabilization to insulin secondary structure, as reflected in the kinetic

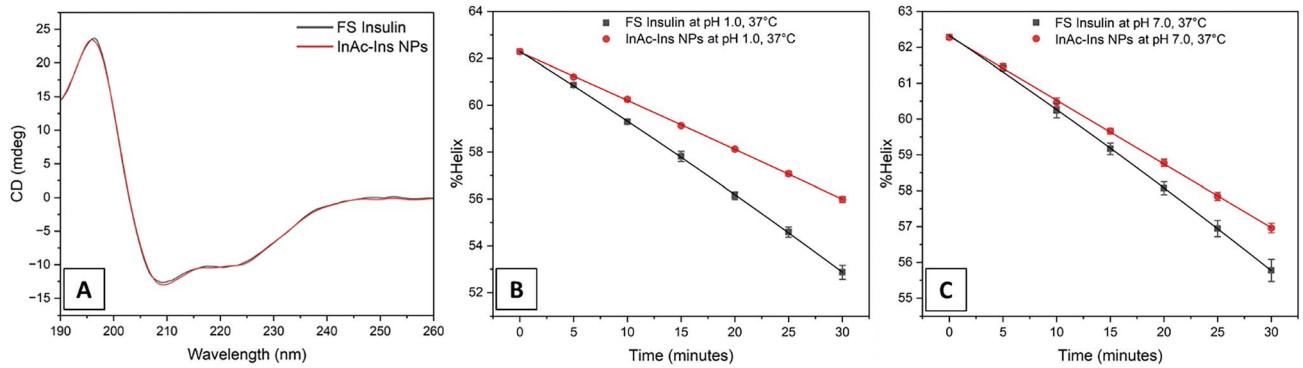

Fig. 5 (A) CD spectra comparing FS insulin and insulin encapsulated within InAc NPs (InAc-Ins NPs). (B) α-Helix content reduction over time for FS insulin and InAc-Ins NPs in simulated gastric fluid (SGF; pH 1, 37 °C) and (C) α-helix content reduction over time for FS insulin and InAc-Ins NPs in simulated small intestinal fluid (SSIF; pH 7, 37 °C). FS insulin shows significantly faster α-helix structure denaturation in SGF compared to InAc-Ins NPs (p-value < 0.05).

Table 2 Comparison of kinetic and thermodynamic studies of insulin secondary structure

Sample	pH	k (min^{-1})	$t_{1/2}$ (min)	($\Delta H^{\ddagger}_{D-N}$) (kcal mol^{-1})	Sources
FS insulin	1	$5.51 \times 10^{-3} \pm 1.97 \times 10^{-4}$	126 ± 5	1.46 ± 0.02	This work
	7	$3.78 \times 10^{-3} \pm 0.82 \times 10^{-4}$	183 ± 4	0.52 ± 0.24	This work
Levan-Ins NPs	1	$6.72 \times 10^{-3} \pm 7.64 \times 10^{-4}$	93 ± 12	1.06 ± 0.32	Kurniawati *et al.*[21]
	7	$7.10 \times 10^{-3} \pm 5.40 \times 10^{-4}$	98 ± 7	3.15 ± 1.93	Kurniawati *et al.*[21]
LevAc-Ins NPs	1	$4.22 \times 10^{-3} \pm 1.43 \times 10^{-4}$	164 ± 6	2.68 ± 0.38	Kurniawati *et al.*[21]
	7	$2.98 \times 10^{-3} \pm 13.2 \times 10^{-4}$	233 ± 10	3.70 ± 0.37	Kurniawati *et al.*[21]
In-Ins NPs	1	$4.12 \times 10^{-3} \pm 1.03 \times 10^{-4}$	168 ± 4	1.75 ± 0.18	Rasjava *et al.*[18]
	7	$3.91 \times 10^{-3} \pm 1.53 \times 10^{-4}$	177 ± 7	1.03 ± 0.02	Rasjava *et al.*[18]
InAc-Ins NPs	1	$3.55 \times 10^{-3} \pm 0.82 \times 10^{-4}$	195 ± 5	4.03 ± 0.21	This work
	7	$2.99 \times 10^{-3} \pm 0.77 \times 10^{-4}$	231 ± 6	1.83 ± 0.18	This work

constant (k), denaturation half-life ($t_{1/2}$), and denaturation transition enthalpy ($\Delta H^{\ddagger}_{D-N}$) at both pH 1 and pH 7 despite both being fructan-type polysaccharides composed of fructose monomers. Notably, InAc-Ins NPs showed the highest stability parameters, with $\Delta H^{\ddagger}_{D-N}$ values of 4.03 ± 0.21 kcal mol^{-1} (pH 1) and 1.83 ± 0.18 kcal mol^{-1} (pH 7). This surpasses both unmodified levan- and inulin-based systems, and even LevAc-Ins NPs which calculated $\Delta H^{\ddagger}_{D-N}$ values of 2.68 ± 0.38 kcal mol^{-1} and 3.70 ± 0.37 kcal mol^{-1} at pH 1 and 7, respectively.

From a structural perspective, these differences can be attributed to the structural distinctions between inulin and levan. Inulin is primarily composed of linear β(2 → 1)-linked fructose units, whereas levan consists of highly branched β(2 → 6)-linked chains.[13,46] Inulin adopts a compact, globular conformation with a higher persistence length, indicating greater rigidity and reduced conformational freedom, while levan exhibit higher flexibility and lower energetic barriers to conformational transitions.[42] These molecular traits influence encapsulation behavior with inulin rigidity and tighter chain packing promote the formation of denser nanoparticle matrices, particularly when acetylated. Acetylation further enhances hydrophobicity and reduces hydrogen bonding capacity,[47] thus limiting water permeability and preserving the α-helical structure of insulin under acidic or neutral conditions. In contrast, the branched structure of levan may form more flexible, solvent-accessible networks that are less effective at protecting the encapsulated insulin from gastrointestinal conditions.[21]

Insulin tertiary structure stability in nanoparticles. The stability of insulin tertiary structure under different conditions was evaluated by monitoring the maximum fluorescence intensity of free and encapsulated insulin at pH 1 and pH 7 at 37 °C. Tyrosine (Tyr) residues within insulin served as intrinsic fluorescence probes to evaluate structural integrity. While the emission wavelength of Tyr remains largely unchanged regardless of solvent polarity, the fluorescence intensity is sensitive to environmental changes. Since insulin denaturation results in fluorescence quenching, the reduction in fluorescence intensity over time was used as an indicator of structural stability.[48] The fluorescence intensity of free insulin declined more rapidly than that of encapsulated insulin at both pH levels, suggesting faster exposure of Tyr residues to the polar environment, thereby accelerating denaturation (Fig. 6 and S4†).[49]

Insulin encapsulation with InAc significantly reduced the rate of fluorescence quenching, thereby prolonging the half-life of insulin tertiary structure stability by approximately threefold compared to FS insulin. These results suggest that inulin encapsulation offers effective protection against pH-induced denaturation (Fig. 6). The E_a value of FS insulin was calculated

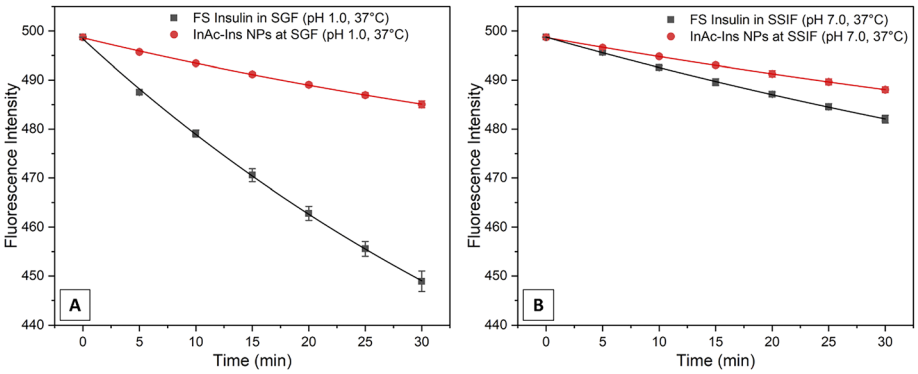

Fig. 6 The decrease of fluorescence intensity over time for FS insulin and encapsulated insulin: (A) InAc-Ins NPs in SGF (pH 1) and (B) InAc-Ins NPs in SSIF (pH 7) while incubated at 37 °C. Tertiary structure denaturation of FS insulin is significantly faster in SGF compared to InAc-Ins NPs (p-value < 0.05).

to be 1.80 ± 0.04 kcal mol^{-1} at pH 1 and 1.11 ± 0.02 kcal mol^{-1} at pH 7. In contrast, insulin encapsulation with InAc resulted in a significant increase in E_a value reaching 19.28 ± 0.05 kcal-mol^{-1} at pH 1 and 5.20 ± 0.25 kcal mol^{-1} at pH 7. Thermodynamic analysis was further conducted to evaluate the insulin structural stability by determining the $\Delta H^{\ddagger}_{D-N}$ value for the tertiary structure. The results showed that insulin encapsulation with InAc significantly increased $\Delta H^{\ddagger}_{D-N}$ by 17.49 ± 0.04 kcal mol^{-1} at pH 1 and 4.09 ± 0.17 kcal mol^{-1} at pH 7. This increase in transition enthalpy indicates a higher energy requirement for denaturation of the encapsulated insulin, further supporting its improved structural stability (Table 3).[18] The observed $\Delta H^{\ddagger}_{D-N}$ increase aligns with previous studies involving insulin encapsulation with acetylated levan (LevAc-insulin NPs), which demonstrated an increase of approximately 2.68 ± 0.38 kcal mol^{-1} in the denaturation energy barrier.[21]

Overall, these results demonstrate that inulin-based encapsulation provides effective protection against pH-induced denaturation by acting as a barrier that shields insulin from external environmental factors. Additionally, acetylation further enhances the protective capability of inulin, as evidenced by the increased stability parameters compared to unacetylated inulin-encapsulated insulin.[21,50]

The comparative data in Table 3 further reinforces this trend when examining insulin tertiary structure stability. InAc-Ins NPs showed a remarkably high $\Delta H^{\ddagger}_{D-N}$ value of 18.67 ± 0.05 kcal mol^{-1} at pH 1 and 4.58 ± 0.25 kcal mol^{-1} at pH 7, compared to LevAc-Ins NPs with $\Delta H^{\ddagger}_{D-N}$ values of 6.28 ± 0.66 and 2.31 ± 1.00 kcal mol^{-1}, respectively. These differences are consistent with the fluorescence intensity decay analysis, where InAc encapsulation significantly prolonged the half-life of insulin tertiary structure by 3.8–4.6 times compared to FS insulin, outperforming all levan-based formulations. These results are consistent with the structural advantages previously described in the context of secondary structure stability, where the linear and hydrophobic nature of InAc contributes to a more confined and water-excluding environment compared to levan-based NPs.[21,42,46] Such features likely also support the improved preservation of insulin tertiary conformation observed here.

Oral glucose tolerance test. To evaluate the impact of insulin-inulin nanoparticles on blood glucose reduction, overnight-fasted mice were randomly assigned to seven groups. The baseline fasting blood glucose level was recorded 82.20 ± 6.71 mg dL^{-1}. The treatment groups received one of the following formulations: subcutaneous insulin (2.5 IU kg^{-1}, SC), In-B nanoparticles (750 mg kg^{-1}, oral), InAc-B nanoparticles (750 mg kg^{-1}, oral), In-Insulin nanoparticles (50 IU kg^{-1}, oral), InAc-Insulin nanoparticles (50 IU kg^{-1}, oral), or free-state (FS) insulin (50 IU kg^{-1}, oral), each dispersed in 1 mL of 0.25% (w/v) sodium carboxymethyl cellulose (Na-CMC). The control group received 1 mL of 0.25% (w/v) Na-CMC alone. Immediately

Table 3 Comparison of the kinetic and thermodynamic studies of insulin in nanoparticles

Sample	pH	k (min^{-1})	$t_{1/2}$ (min)	($\Delta H^{\ddagger}_{D-N}$) (kcal mol^{-1})	Sources
FS insulin	1	$3.47 \times 10^{-3} \pm 5.00 \times 10^{-5}$	199 ± 11	1.18 ± 0.03	This work
	7	$1.13 \times 10^{-3} \pm 5.24 \times 10^{-5}$	611 ± 40	0.49 ± 0.02	This work
Levan-Ins NPs	1	$1.62 \times 10^{-2} \pm 1.47 \times 10^{-3}$	43 ± 4	2.18 ± 0.33	Kurniawati *et al.*[21]
	7	$1.21 \times 10^{-2} \pm 1.40 \times 10^{-3}$	58 ± 7	3.37 ± 0.55	Kurniawati *et al.*[21]
LevAc-Ins NPs	1	$3.97 \times 10^{-3} \pm 3.92 \times 10^{-4}$	175 ± 17	6.28 ± 0.66	Kurniawati *et al.*[21]
	7	$4.41 \times 10^{-3} \pm 5.41 \times 10^{-4}$	159 ± 20	2.31 ± 1.00	Kurniawati *et al.*[21]
In-Ins NPs	1	$2.37 \times 10^{-3} \pm 4.29 \times 10^{-5}$	291 ± 24	2.71 ± 0.21	Rasjava *et al.*[18]
	7	$1.05 \times 10^{-3} \pm 4.74 \times 10^{-5}$	657 ± 37	0.69 ± 0.13	Rasjava *et al.*[18]
InAc-Ins NPs	1	$0.63 \times 10^{-3} \pm 0.24 \times 10^{-5}$	765 ± 34	18.67 ± 0.05	This work
	7	$0.75 \times 10^{-3} \pm 0.23 \times 10^{-5}$	919 ± 27	4.58 ± 0.25	This work

following the treatment, all mice were orally administered glucose at a dose of 3 g kg^{-1} body weight.

Distinct post-glucose administration glycemic profiles were observed across treatment groups. The control group exhibited peak blood glucose levels at 60 minutes post-glucose administration, while the treated groups reached peak blood glucose levels earlier at 30 minutes. Both In-Ins and InAc-Ins NPs significantly reduce blood glucose levels relative to the control group (p-value < 0.05), with InAc-Ins NPs exhibiting the most notable effect (Fig. 7A).

Analysis of glucose intolerance *via* area under the curve (AUC) revealed that FS insulin did not significantly alter glycemic response compared to the control, confirming previous observations of the limited efficacy of unencapsulated oral insulin.[18] In contrast, AUC values in both the In-Ins and InAc-Ins groups were significantly lower than in the control (p-value < 0.05), indicating a significant hypoglycemic effect (Fig. 7B). These outcomes are consistent with prior reports suggesting that inulin encapsulation enhances insulin oral bioavailability and pharmacodynamic profile.[21] Although inulin itself has been reported to exert a mild glucose-lowering effect,[51] neither In-B nor InAc-B NPs induced significant glycemic changes, suggesting that the observed hypoglycemic effects in insulin-loaded groups were solely due to insulin and not the inulin carrier matrix. Quantitative comparisons demonstrated that In-Ins NPs achieved approximately 31.48% of the glucose-lowering efficacy of SC insulin, whereas InAc-Ins NPs achieved 42.80%, representing a 23.77% improvement over In-Ins NPs. This enhancement is likely attributable to the sustained release and improved structural stability by InAc NPs.

To further explore the dose responsiveness of InAc-Ins NPs, additional groups received increasing doses of 50, 100, and 200 IU kg^{-1}, corresponding to D1, D2, and D4 groups, respectively (Fig. 7C and D). All dose groups exhibited a similar glucose-lowering trend, with blood glucose levels peaking at 30 minutes and returning toward baseline over time. AUC values for all InAc-Ins dose groups were significantly reduced compared to the control, confirming the glucose-lowering potential of this formulation (p-value < 0.05). These findings are consistent with previous studies that suggest a dose-

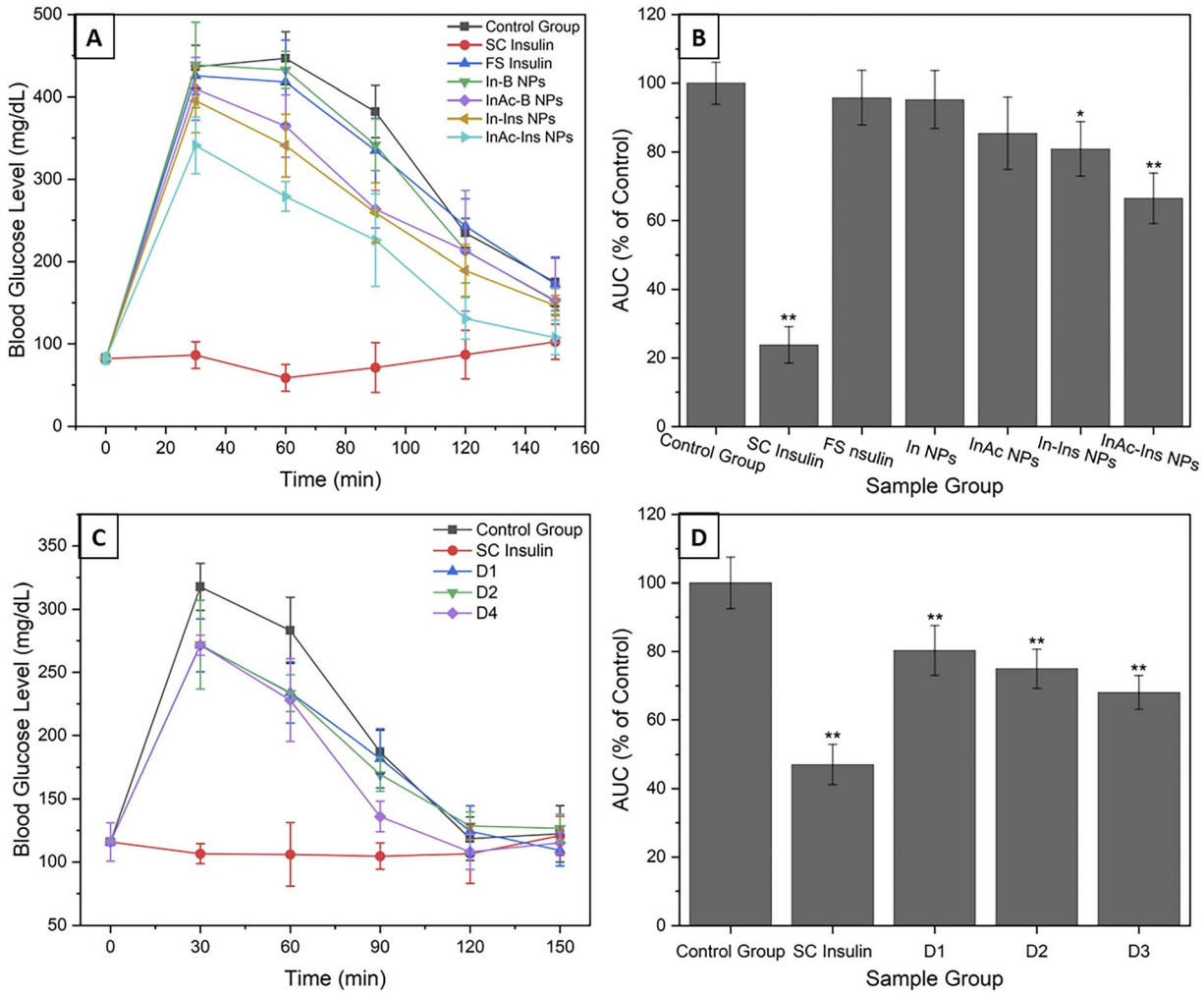

Fig. 7 The effects of inulin-insulin nanoparticles on normal mice. (A) Glucose levels of different treatment groups, (B) glucose levels of different treatment dosage groups, and (C and D) quantification of the AUC, depicted as percentage relative to the control value. *p-value < 0.05 compared to control group.

dependent enhancement in blood glucose reduction.[52] However, no statistically significant differences were observed between the three dosing groups (p-value > 0.05), suggesting the presence of a dose plateau effect (Fig. 7D). This phenomenon likely reflects saturation of insulin absorption or receptor-mediated activity, where further increases in administered insulin do not yield proportional enhancements in pharmacological effect.[53]

These findings demonstrate that InAc-Ins NPs not only enhance oral insulin delivery and glycemic control relative to FS insulin and In-Ins NPs, but also achieve relevant efficacy at a moderate dose. However, the lack of significant differentiation at higher doses indicates the need for further investigation into dose optimization and long-term glycemic effect.

To better understand the underlying mechanism behind this hypoglycemic efficacy, the following discussion considers the conditions of the nanoparticles and insulin along the gastrointestinal tract. The InAc-Ins nanoparticle system was designed for colon-targeted release and absorption of insulin. The InAc matrix provides protection against acidic pH and proteolytic enzymes in the stomach and small intestine, minimizing insulin degradation during upper GI transit. Upon reaching lower intestine, bifidobacteria and other inulin-fermenting microbiota enzymatically cleave the inulin backbone, facilitating the microbial-triggered release of insulin at the lower intestine.[54]

The released insulin is presumed to be absorbed as a free peptide, rather than as intact nanoparticles. Although the lower intestine is considered less permeable, recent studies support its potential as a viable absorption site for macromolecules.[55] The colon exhibits several favorable features including neutral pH, low protease activity, long residence time, and a mucosal barrier with modifiable tight junctions, which can allow paracellular and transcytotic transport of peptides.[56,57] This hypothesis is supported by the observed *in vivo* hypoglycemic effect, suggesting successful systemic delivery of bioactive insulin.

Conclusions

This study successfully demonstrates the development of a novel oral insulin delivery system using acetylated inulin nanoparticles synthesized from *Salinivibrio* sp. GM01. Acetylation significantly enhanced the physicochemical properties of inulin, improving its hydrophobicity, reducing particle size, and increasing insulin encapsulation efficiency. The engineered nanoparticles provided sustained insulin release under simulated gastrointestinal conditions, effectively minimizing the burst release observed in non-acetylated inulin carriers. Biophysical evaluations showed that acetylated inulin nanoparticles significantly improved insulin structural stability by increasing its denaturation half-life and activation energy, both for the secondary and tertiary structures level. Moreover, *in vivo* oral glucose tolerance tests confirmed the hypoglycemic efficacy of the encapsulated insulin. The InAc-Ins NPs successfully achieving up to 42.8% of subcutaneous insulin activity and showing a promising dose-dependent response. Collectively, these findings suggest that InAc NPs offer a biocompatible, non-invasive, and effective platform for oral insulin delivery, with potential applications in improving patient compliance in DM therapy.

Data availability

The data supporting this article have been included as part of the ESI.†

Author contributions

Achmad Ramadhanna'il Rasjava: conceptualization, methodology, investigation, formal analysis, data curation, visualization, writing – original draft, project administration. Rukman Hertadi: conceptualization, supervision, resources, writing – review & editing, funding acquisition. Neng Fisheri Kurniati: methodology, Investigation (*in vivo* studies and formulation), validation, supervision, writing – review & editing. All authors have read and agreed to the published version of the manuscript.

Conflicts of interest

The authors declare no conflicts of interest in relation to this work. There are no financial or personal relationships that could be viewed as potential competing interests.

Acknowledgements

This research was funded by the Doctoral Thesis Research Grant from Kementerian Pendidikan, Kebudayaan, Riset, dan Teknologi, Indonesia under grant number 266/IT1.B07.1/SPP-LPPM/V/2022. The authors express their sincere gratitude to Dr Elvira Hermawati, Head of the Chemical Instrument Laboratory, Faculty of Mathematics and Natural Sciences, Bandung Institute of Technology, for the assistance in conducting the circular dichroism spectral measurements. The authors also extend their appreciation to the Biophysics and Biomaterials Research Group for providing the bacterial strains used in this study.

References

1 S. A. Antar, N. A. Ashour, M. Sharaky, M. Khattab, N. A. Ashour, R. T. Zaid, E. J. Roh, A. Elkamhawy and A. A. Al-Karmalawy, *Biomed. Pharmacother.*, 2023, **168**, 115734.
2 D. Mauricio, M. Gratacòs and J. Franch-Nadal, *Cardiovasc. Diabetol.*, 2023, **22**, 1–21.
3 Y. Xiao, Z. Tang, J. Wang, C. Liu, N. Kong, O. C. Farokhzad and W. Tao, *Angew. Chem., Int. Ed.*, 2020, **59**, 19787–19795.
4 Y. Zhang, J. Yu, A. R. Kahkoska, J. Wang, J. B. Buse and Z. Gu, *Adv. Drug Delivery Rev.*, 2019, **139**, 51–70.
5 G. Iyer, S. Dyawanapelly, R. Jain and P. Dandekar, *Int. J. Biol. Macromol.*, 2022, **208**, 565–585.

6 S. Mitragotri, P. A. Burke and R. Langer, *Nat. Rev. Drug Discovery*, 2014, **13**, 655–672.
7 S. Spoorthi Shetty, P. Halagali, A. P. Johnson, K. M. A. Spandana and H. V. Gangadharappa, *Int. J. Biol. Macromol.*, 2023, **242**, 125114.
8 J. K. Patra, G. Das, L. F. Fraceto, E. V. R. Campos, M. D. P. Rodriguez-Torres, L. S. Acosta-Torres, L. A. Diaz-Torres, R. Grillo, M. K. Swamy, S. Sharma, S. Habtemariam and H. S. Shin, *J. Nanobiotechnol.*, 2018, **16**, 1–33.
9 E. B. Souto, S. B. Souto, J. R. Campos, P. Severino, T. N. Pashirova, L. Y. Zakharova, A. M. Silva, A. Durazzo, M. Lucarini, A. A. Izzo and A. Santini, *Molecules*, 2019, **24**, 1–29.
10 Y. Han, J. Spicer, Y. Huang, C. Bunt, M. Liu and J. Wen, *Eur. J. Lipid Sci. Technol.*, 2024, **126**, 1–15.
11 Y. K. Sung and S. W. Kim, *Biomater. Res.*, 2020, **24**, 12.
12 I. Karimi, M. Ghowsi, L. J. Mohammed, Z. Haidari, K. Nazari and H. B. Schiöth, *Polymers*, 2025, **17**(3), 412.
13 W. Sheng, G. Ji and L. Zhang, *Front. Immunol.*, 2023, **14**, 1–16.
14 A. Wasim, J. Ramakant and G. Navneet, *J. Drug Delivery Ther.*, 2019, **9**, 437–441.
15 F. Afinjuomo, S. Abdella, S. H. Youssef, Y. Song and S. Garg, *Pharmaceuticals*, 2021, **14**(9), 855.
16 X. Y. Wu and P. I. Lee, *J. Appl. Polym. Sci.*, 2000, **77**, 833–840.
17 M. Walz, T. Hirth and A. Weber, *Colloids Surf., A*, 2018, **536**, 47–52.
18 A. R. Rasjava, D. Kurniawati, W. O. S. Rizki, N. F. Kurniati and R. Hertadi, *J. Biomater. Sci., Polym. Ed.*, 2025, **36**, 963–986.
19 K. L. Zapadka, F. J. Becher, A. L. Gomes dos Santos and S. E. Jackson, *Interface Focus*, 2017, **7**(6), 20170030.
20 Y. Han, S. Yu, L. Liu, S. Zhao, T. Yang, Y. Yang, Y. Fang and S. Lv, *Mol. Catal.*, 2018, **457**, 24–32.
21 D. Kurniawati, N. F. Kurniati, E. Ratnaningsih and R. Hertadi, *Biomed. Mater.*, 2025, **20**, 25028.
22 A. K. Jain, V. Sood, M. Bora, R. Vasita and D. S. Katti, *Carbohydr. Polym.*, 2014, **112**, 225–234.
23 E. Budianto and S. H. Astuti, *Global J. Environ. Sci. Manage.*, 2020, **6**, 523–536.
24 H. Ünal, N. Öztürk and E. Bilensoy, *Beilstein J. Org. Chem.*, 2015, **11**, 204–212.
25 T. C. Coutinho, P. W. Tardioli and C. S. Farinas, *Appl. Biochem. Biotechnol.*, 2020, **190**, 270–292.
26 K. K. Yadav, M. Ojha, R. Pariary, M. Arakha, A. Bhunia and S. Jha, *Biochimie*, 2022, **193**, 64–77.
27 K. Takahashi, Y. Kitaoka and H. Hatta, *J. Physiol. Sci.*, 2024, **74**, 32.
28 A. Bhanja, S. K. Paikra, P. P. Sutar and M. Mishra, *J. Food Sci. Technol.*, 2023, **60**, 328–339.
29 D. Ni, S. Zhang, O. Klrtel, W. Xu, Q. Chen, E. T. Öner and W. Mu, *J. Agric. Food Chem.*, 2021, **69**, 13125–13134.
30 W. M. El-Kholy, R. A. Aamer and A. N. A. Ali, *Ann. Agric. Sci.*, 2020, **65**, 59–67.
31 B. Hufnagel, V. Muellner, K. Hlatky, C. Tallian, R. Vielnascher, G. M. Guebitz, M. Wirth and F. Gabor, *Carbohydr. Polym.*, 2021, **252**, 117091.
32 N. Petkova, G. Gencheva, D. Vassilev, M. Koleva, A. Krastanov and P. Denev, *J. Renewable Mater.*, 2018, **6**, 671–679.
33 V. D. Trela, A. L. Ramallo and O. A. Albani, *Braz. Arch. Biol. Technol.*, 2020, **63**, 1–13.
34 L. A. Bello-Pérez, E. Agama-Acevedo, P. B. Zamudio-Flores, G. Mendez-Montealvo and S. L. Rodriguez-Ambriz, *LWT*, 2010, **43**, 1434–1440.
35 M. Feng and P. Li, *J. Biomed. Mater. Res., Part A*, 2007, **80A**, 184–193.
36 N. Qin, Y. Li, L. Zhang, L. Guo, W. Zhang, G. Li and J. Bai, *RSC Adv.*, 2024, **14**, 23037–23047.
37 S. Yu, G. Peng and D. Wu, *Int. J. Biol. Macromol.*, 2024, **254**, 127883.
38 J. H. Xie, F. Zhang, Z. J. Wang, M. Y. Shen, S. P. Nie and M. Y. Xie, *Carbohydr. Polym.*, 2015, **133**, 596–604.
39 Z. Hu, J. Sun, L. Jin, T. Zong, Y. Duan, H. Zhou, W. Zhou and G. Li, *Polymers*, 2022, **14**(15), 3130.
40 Z. Huang, M. H. Zong and W. Y. Lou, *Food Hydrocolloids*, 2022, **124**, 107217.
41 H. Wu, Z. Cui, Y. Huo, Y. Sun, X. Zhang, J. Guan and S. Mao, *J. Pharm. Sci.*, 2021, **110**, 2800–2807.
42 K. Nester and W. Plazinski, *Carbohydr. Polym.*, 2020, **240**, 116266.
43 M. Walz, D. Hagemann, M. Trentzsch, A. Weber and T. Henle, *Carbohydr. Polym.*, 2018, **199**, 102–108.
44 Y. A. B. Neolaka, Y. Lawa, M. Riwu, H. Darmokoesoemo, H. Setyawati, J. Naat, B. Ayu Widyaningrum, U. Osagie Aigbe, K. Eghonghon Ukhurebor, R. Birundu Onyancha and H. S. Kusuma, *Results Chem.*, 2022, **4**, 100578.
45 W. J. Kim, Y. J. Kwon, C. H. Cho, S. K. Ye and K. O. Kim, *Sci. Rep.*, 2021, **11**, 1–13.
46 A. Miranda-Molina, S. Castrejón-Carrillo, G. T. Zavala-Padilla, M. Antúnez-Mojica, L. Alvarez, M. E. Rodríguez-Alegría and A. L. Munguía, *Carbohydr. Polym.*, 2025, **352**, 123236.
47 K. T. Araoye, S. A. Akinola, A. M. Oyelade, S. Ogagar, M. B. Oyewale, E. M. Ogunbusola, T. A. Sanni and O. F. Oludahunsi, *Food Humanit.*, 2024, **2**, 100237.
48 A. Kumar and P. Venkatesu, *RSC Adv.*, 2014, **4**, 4487–4499.
49 V. Sundaram, R. N. Ramanan, M. Selvaraj, R. Vijayaraghavan, D. R. MacFarlane and C. W. Ooi, *Int. J. Biol. Macromol.*, 2022, **208**, 544–552.
50 Y. Chen, P. Li, J. A. Modica, R. J. Drout and O. K. Farha, *J. Am. Chem. Soc.*, 2018, **140**, 5678–5681.
51 T. F. Teferra, *Food Front.*, 2021, **2**, 407–416.
52 O. Horakova, P. Kroupova, K. Bardova, J. Buresova, P. Janovska, J. Kopecky and M. Rossmeisl, *Sci. Rep.*, 2019, **9**, 1–11.
53 M. S. Salahudeen and P. S. Nishtala, *Saudi Pharm. J.*, 2017, **25**, 165–175.
54 F. Guo, T. Ouyang, T. Peng, X. Zhang, B. Xie, X. Yang, D. Liang and H. Zhong, *Biomater. Sci.*, 2019, **7**, 1493–1506.
55 S. H. Lee, S. Y. Back, J. G. Song and H. K. Han, *J. Nanobiotechnol.*, 2020, **18**, 1–10.
56 M. Katsuma, S. Watanabe, H. Kawai, S. Takemura and K. Sako, *Int. J. Pharm.*, 2006, **307**, 156–162.
57 S. Seyam, H. Choukaife, O. Al Rahal and M. Alfatama, *Int. J. Biol. Macromol.*, 2024, **281**, 136549.